On Relation Between Leakage-Free Condition and Differential Filtering Order in ETFE-Based Frequency Responce Function Estimation*

Yoshihiro Maeda[1], Taishi Yazawa[1], Shimpei Sato[1], and Wataru Hara[1]

***Abstract*— Estimation of an accurate frequency response function (FRF) of a target system is crucial to design fine servo controllers that realize fast and precise positioning control. The empirical transfer function estimation (ETFE) is the most representative and simplest FRF estimation method in terms of industrial utility. However, its applicability is limited to input and output signals of a target system measured during periodic or reciprocating operations, due to leakage errors induced by the discrete Fourier transform. Recently, an FRF estimation method combining ETFE with differential filtering has been proposed, which enables accurate FRF estimation in point-to-point motion. This paper theoretically clarifies the relationship between leakage-free condition and the differential filtering order in the ETFE-based FRF estimation framework. Furthermore, it is demonstrated through simulations that increasing the differential filtering order can broaden the input and output signals acquisition conditions that enables accurate FRF estimation.**

I. Introduction

A variety of industrial mechatronics equipment, including that used for manufacturing electrical components and semiconductors, is experiencing increasing demand for faster and more precise positioning mechanisms. This demand is driven by the need for improved quality and productivity [1], [2]. The frequency response function (FRF) of a target system is a valuable non-parametric model for not only system analysis but also designing high-precision positioning controllers [3]. Accurate estimation of the FRF is a critical aspect of the control design process that significantly impacts control performance [4], [5], [6].

The empirical transfer function estimation (ETFE) is a widely used method for estimating the FRF in the industry, favored for its simplicity and effectiveness [7], [8]. It involves calculating the FRF estimate from the ratio of the discrete Fourier transform (DFT) of input and output signals of a target system. However, due to its reliance on the DFT, the aperiodicity of input and output signals can introduce leakage errors, deteriorating the accuracy of FRF estimation. As a result, ETFE is typically employed with periodic input and output signals or signals whose initial and final states coincide, such as in reciprocating motion. Recently, local frequency modeling [9], [10] has emerged as an alternative method for estimating the FRF that is not constrained by the periodicity or the reciprocity in input and output signals. This approach, which assumes the smoothness of the true FRF within a local frequency band, uses a parametric modeling technique to estimate the system FRF separately from leakage errors. However, to effectively facilitate the separate estimation, system identification tests using additional excitation by multi-sine or random-noise signals are required. This implies that it is unable to perform FRF estimation directly from the input and output signals measured during processing operations of mechatronics systems. If the system FRF can be accurately estimated without interrupting the processing operations for system identification, it becomes possible to perform tasks such as controller adjustments and diagnosing anomalies in the positioning mechanism more frequently [11], [12].

To address this limitation, the authors proposed a method called ETFE-Diff (empirical transfer function estimation with differential filtering) [13], which allowed for FRF estimation from point-to-point (PTP) positioning motion signals measured during actual operation. This technique, which employs a first-order differential filter to compute the differential input and output signals for the DFT-based FRF estimation, offers a straightforward alternative to traditional ETFE. By modifying the leakage-free condition through differential filtering, ETFE-Diff facilitates accurate FRF estimation using not only periodic and reciprocating motion signals but also PTP motion signals. In addition, by applying this method to controller design, improved positioning accuracy under plant perturbations and enhanced modeling-free learning are realized in references [13] and [14].

In this study, we have extended the research on ETFE-Diff, demonstrating that by increasing the differential filtering order, the leakage-free condition can be expanded, enabling accurate FRF estimation under a broader range of operating conditions. Specifically, we have newly constructed ETFE with second-order differential filtering, referred to as ETFE-2Diff, and conducted the aforementioned investigation. The key contributions of this study are outlined as follows:

- The leakage-free condition for ETFE-2Diff is theoretically derived and the operating conditions under which leakage errors can be removed are identified, comparing to the existing ETFE and ETFE-Diff.
- Through FRF estimation simulations conducted on a galvano scanner, it is demonstrated that ETFE-2Diff can effectively perform FRF estimation while suppressing leakage errors in various types of motion, including reciprocating, PTP, and ramp motions.

*This work was supported in part by Via Mechanics, Ltd.

[1]Yoshihiro Maeda, Taishi Yazawa, Shimpei Sato, and Wataru Hara are with Electrical and Mechanical Engineering Program, Department of Engineering, Nagoya Institute of Technology, 4668555 Nagoya, Japan ymaeda@nitech.ac.jp

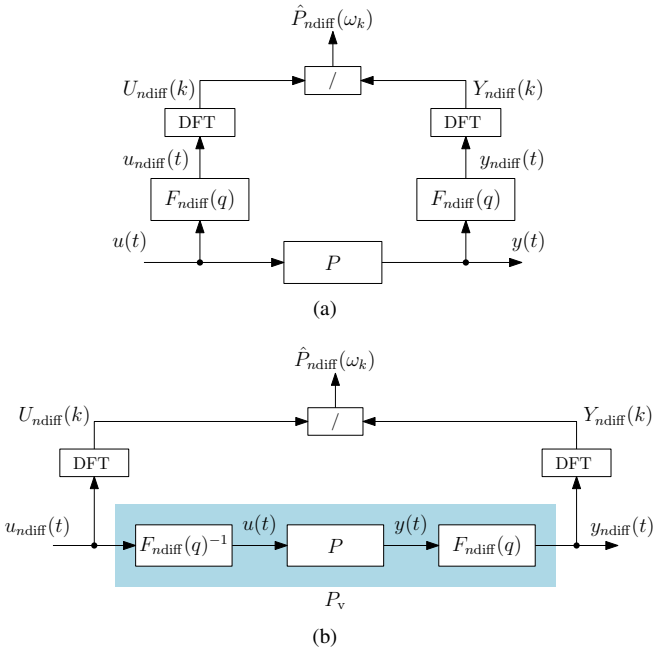

Fig. 1. Block diagram of FRF estimation system: (a) real; (b) virtual.

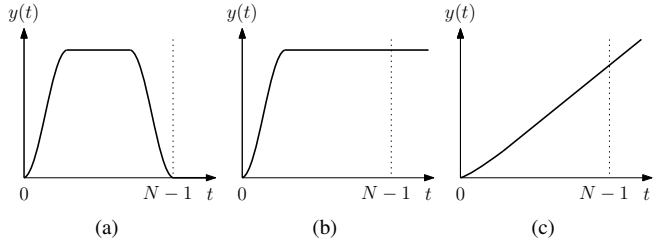

Fig. 2. Conceptual waveform of positioning motion: (a) reciprocating; (b) PTP; (c) ramp.

II. Problem Statement of FRF Estimation

The FRF estimation problem addressed in this study considers the calculation of plant FRF estimate $\hat{P}_{n\mathrm{diff}}(\omega_k)$ from the input and output signals $u(t), y(t)$ of plant P, which is an N_{p}-dimensional linear time-invariant SISO system, as shown in Fig. 1(a). In this figure, t is the index representing discrete time, k is the index representing the discrete frequency, ω_k is the discrete frequency corresponding to k, $u_{n\mathrm{diff}}(t)$ is the n-th differential value of input $u(t)$, $y_{n\mathrm{diff}}(t)$ is the n-th differential value of output $y(t)$, $U_{n\mathrm{diff}}(k)$ is the DFT of $u_{n\mathrm{diff}}(t)$, $Y_{n\mathrm{diff}}(k)$ is the DFT of $y_{n\mathrm{diff}}(t)$, and q is the shift operator. In addition, $F_{n\mathrm{diff}}(q)$ is the n-th order differential filter defined by

$$F_{n\mathrm{diff}}(q) = (1 - q^{-1})^n \tag{1}$$

Define the DFT $G(k)$ of time signal $g(t), t = 0, 1, \ldots, N-1$ by the following equation:

$$G(k) = \sum_{t=0}^{N-1} g(t) e^{-j\frac{2\pi kt}{N}}, \ k = 0, 1, ..., N-1 \tag{2}$$

where, the discrete frequency index k and the discrete frequency ω_k have the correspondence $\omega_k = 2\pi k / NT_{\mathrm{s}}$ (where T_{s} is the sampling period).

TABLE I

Assumption in each motion pattern.

Motion pattern	Assumption
Recip.	i) $\boldsymbol{x}_{\mathrm{p}}(t \le 0) = \boldsymbol{x}_{\mathrm{p}}(t \ge N-2)$
PTP	i) $\boldsymbol{x}_{\mathrm{p}}(t < 0) = \boldsymbol{x}_{\mathrm{p}}(0)$, ii) $\boldsymbol{x}_{\mathrm{p}}(t > N-2) = \boldsymbol{x}_{\mathrm{p}}(N-2)$
Ramp	i) $\boldsymbol{x}_{\mathrm{p}}(t < 0) = \boldsymbol{x}_{\mathrm{p}}(0)$, ii) $\boldsymbol{x}_{\mathrm{p}}(N) - \boldsymbol{x}_{\mathrm{p}}(N-1)$ $= \boldsymbol{x}_{\mathrm{p}}(N-1) - \boldsymbol{x}_{\mathrm{p}}(N-2)$

The state-space representation of plant P is defined by the following equation:

$$P : \begin{cases} \boldsymbol{x}_{\mathrm{p}}(t+1) = \boldsymbol{A}_{\mathrm{p}} \boldsymbol{x}_{\mathrm{p}}(t) + \boldsymbol{B}_{\mathrm{p}} u(t) \\ y(t) = \boldsymbol{C}_{\mathrm{p}} \boldsymbol{x}_{\mathrm{p}}(t) \end{cases} \tag{3}$$

where $\boldsymbol{x}_{\mathrm{p}}(t) \in \mathbb{R}^{N_{\mathrm{p}}}$ is the state vector at discrete time t, $\boldsymbol{A}_{\mathrm{p}} \in \mathbb{R}^{N_{\mathrm{p}} \times N_{\mathrm{p}}}, \boldsymbol{B}_{\mathrm{p}} \in \mathbb{R}^{N_{\mathrm{p}} \times 1}, \boldsymbol{C}_{\mathrm{p}} \in \mathbb{R}^{1 \times N_{\mathrm{p}}}$ are the state matrices. According to (3), the discrete-time Fourier transform $P(\omega_k)$ is expressed by

$$P(\omega_k) = \boldsymbol{C}_{\mathrm{p}} (e^{j\omega_k} \boldsymbol{I} - \boldsymbol{A}_{\mathrm{p}})^{-1} \boldsymbol{B}_{\mathrm{p}} \tag{4}$$

In this study, the estimate $\hat{P}_{n\mathrm{diff}}(\omega_k)$ is calculated in the FRF estimation system depicted in Fig. 1(a) by using the input and output signals $u(t), y(t), t = 0, 1, \ldots, N-1$ for the positioning motion patterns of reciprocating, PTP, and ramp motions shown in Fig. 2. It is assumed that the input and output signals are in a stable state at times $t \le 0, t \ge N-2$ for any of the motion pattern, and the plant state $\boldsymbol{x}_{\mathrm{p}}(t)$ at those times satisfies the conditions in Table I.

III. Leakage-Free Condition in ETFE Method Using Differential Filtering

In this section, the leakage-free condition for ETFE combined with differential filtering is theoretically derived with differential filtering orders of $n = 0, 1$, and 2 according to the problem statement established in Sect. II.

A. ETFE ($n = 0$)

ETFE is the case of $n = 0$, i.e., without using differential filters, and the DFT $Y(k) (= Y_{0\mathrm{diff}}(k))$ of the output $y(t) (= y_{0\mathrm{diff}}(t))$ in (3) can be expressed as follows [7], [9]:

$$\begin{aligned} Y(k) &= P(\omega_k) U(k) + T(\omega_k) \\ T(\omega_k) &= \boldsymbol{C}_{\mathrm{p}} \left(e^{j\omega_k} \boldsymbol{I} - \boldsymbol{A}_{\mathrm{p}}\right)^{-1} e^{j\omega_k} \{\boldsymbol{x}_{\mathrm{p}}(0) - \boldsymbol{x}_{\mathrm{p}}(N)\} \end{aligned} \tag{5}$$

where $U(k) (= U_{0\mathrm{diff}}(k))$ is the DFT of $u(t) (= u_{0\mathrm{diff}}(t))$ and $T(\omega_k)$ represents the leakage errors in ETFE. The plant FRF estimate in ETFE is expressed by the following equation:

$$\hat{P}_{0\mathrm{diff}}(\omega_k) := \frac{Y(k)}{U(k)} = P(\omega_k) + \frac{T(\omega_k)}{U(k)} \tag{6}$$

From (5) and (6), the leakage-free condition in ETFE, where $T(\omega_k) = 0$, thus ensuring $\hat{P}_{0\mathrm{diff}}(\omega_k) = P(\omega_k)$, can be expressed as

$$\boldsymbol{x}_{\mathrm{p}}(0) = \boldsymbol{x}_{\mathrm{p}}(N) \tag{7}$$

From (7), it can be understood that ETFE relates to the plant state at $t = 0$ and $t = N$.

B. ETFE-Diff ($n = 1$)

ETFE-Diff is applied for differential filtering order $n = 1$. When (1) and (3) are considered, the DFT $Y_{1\mathrm{diff}}(k)$ of the first-order differential output $y_{1\mathrm{diff}}(t)$ is expressed as follows [13]:

$$\begin{aligned} Y_{1\mathrm{diff}}(k) &= P(\omega_k)U_{1\mathrm{diff}}(k) + T_{1\mathrm{diff}}(\omega_k) \\ T_{1\mathrm{diff}}(\omega_k) &= \boldsymbol{C}_\mathrm{p}\left(e^{j\omega_k}\boldsymbol{I} - \boldsymbol{A}_\mathrm{p}\right)^{-1} e^{j\omega_k} \\ &\quad [\{\boldsymbol{x}_\mathrm{p}(0) - \boldsymbol{x}_\mathrm{p}(N)\} \\ &\quad -\{\boldsymbol{x}_\mathrm{p}(-1) - \boldsymbol{x}_\mathrm{p}(N-1)\}] \end{aligned} \tag{8}$$

where $U_{1\mathrm{diff}}(k)$ is the DFT of the first-order differential input $u_{1\mathrm{diff}}(t)$ and $T_{1\mathrm{diff}}(\omega_k)$ represents the leakage errors in ETFE-Diff. The plant FRF estimate in ETFE-Diff is expressed as

$$\hat{P}_{1\mathrm{diff}}(\omega_k) := \frac{Y_{1\mathrm{diff}}(k)}{U_{1\mathrm{diff}}(k)} = P(\omega_k) + \frac{T_{1\mathrm{diff}}(\omega_k)}{U_{1\mathrm{diff}}(k)} \tag{9}$$

According to (8) and (9), the leakage-free condition in ETFE-Diff, where $T_{1\mathrm{diff}}(\omega_k) = 0$, thus $\hat{P}_{1\mathrm{diff}}(\omega_k) = P(\omega_k)$ holds, is expressed by the following equation:

$$\boldsymbol{x}_\mathrm{p}(0) - \boldsymbol{x}_\mathrm{p}(N) = \boldsymbol{x}_\mathrm{p}(-1) - \boldsymbol{x}_\mathrm{p}(N-1) \tag{10}$$

Compared to the leakage-free condition of ETFE as shown in (7), the plant states involved in ETFE-Diff increase to four: $t = -1, 0, N-1, N$. Specifically, it satisfies $T_{1\mathrm{diff}}(\omega_k) = 0$ when the first-order differential values of the plant state (in the case of backward differential) physically match at $t = 0$ and $t = N$. Furthermore, (7) in ETFE represents one of the conditions of (10). For a detailed theoretical representation of the leakage-free condition in ETFE-Diff, see reference [13].

C. ETFE-2Diff ($n = 2$)

In this subsection, the derivation process of the leakage-free condition in ETFE-2Diff, which is applied for differential filtering order $n = 2$, is clarified in detail. To make the mathematical development more comprehensible, consider a virtual plant P_v with integration and differential filters placed before and after the plant P, as depicted in Fig. 1(b), by equivalently transforming Fig. 1(a). In this case, original $u(t)$ can be represented by using the second-order differential input $u_{2\mathrm{diff}}(t)$ of $u(t)$ as follows:

$$\begin{aligned} u(t) &= u_{2\mathrm{diff}}(t) + 2u(t-1) - u(t-2) \\ u_{2\mathrm{diff}}(t) &= (1-q^{-1})^2 u(t) = u(t) - 2u(t-1) + u(t-2) \end{aligned} \tag{11}$$

When (11) is substituted into (3), the following equation is obtained:

$$\begin{aligned} \boldsymbol{x}_\mathrm{p}(t+1) &= \boldsymbol{A}_\mathrm{p}\boldsymbol{x}_\mathrm{p}(t) + \boldsymbol{B}_\mathrm{p}\{u_{2\mathrm{diff}}(t) \\ &\quad + 2u(t-1) - u(t-2)\} \\ &= (\boldsymbol{A}_\mathrm{p} + 2\boldsymbol{I})\boldsymbol{x}_\mathrm{p}(t) - (2\boldsymbol{A}_\mathrm{p} + \boldsymbol{I})\boldsymbol{x}_\mathrm{p}(t-1) \\ &\quad + \boldsymbol{A}_\mathrm{p}\boldsymbol{x}_\mathrm{p}(t-2) + \boldsymbol{B}_\mathrm{p}u_{2\mathrm{diff}}(t) \end{aligned} \tag{12}$$

In addition, the second-order differential output $y_{2\mathrm{diff}}(t)$ of $y(t)$ is expressed by the following equation according to (3):

$$\begin{aligned} y_{2\mathrm{diff}}(t) &= (1-q^{-1})^2 y(t) \\ &= \boldsymbol{C}_\mathrm{p}\{\boldsymbol{x}_\mathrm{p}(t) - 2\boldsymbol{x}_\mathrm{p}(t-1) + \boldsymbol{x}_\mathrm{p}(t-2)\} \end{aligned} \tag{13}$$

From (12) and (13), the state-space representation of the virtual plant P_v with input $u_{2\mathrm{diff}}(t)$ and output $y_{2\mathrm{diff}}(t)$ can be defined as follows:

$$P_\mathrm{v} : \begin{cases} \boldsymbol{x}_\mathrm{vp}(t+1) = \boldsymbol{A}_\mathrm{vp}\boldsymbol{x}_\mathrm{vp}(t) + \boldsymbol{B}_\mathrm{vp}u_{2\mathrm{diff}}(t) \\ y_{2\mathrm{diff}}(t) = \boldsymbol{C}_\mathrm{vp}\boldsymbol{x}_\mathrm{vp}(t) \end{cases} \tag{14}$$

where

$$\begin{aligned} \boldsymbol{x}_\mathrm{vp}(t) &= \begin{bmatrix} \boldsymbol{x}_\mathrm{p}(t) & \boldsymbol{x}_\mathrm{p}(t-1) & \boldsymbol{x}_\mathrm{p}(t-2) \end{bmatrix}^\top \\ \boldsymbol{A}_\mathrm{vp} &= \begin{bmatrix} \boldsymbol{A}_\mathrm{p} + 2\boldsymbol{I} & -2\boldsymbol{A}_\mathrm{p} - \boldsymbol{I} & \boldsymbol{A}_\mathrm{p} \\ \boldsymbol{I} & O & O \\ O & \boldsymbol{I} & O \end{bmatrix} \\ \boldsymbol{B}_\mathrm{vp} &= \begin{bmatrix} \boldsymbol{B}_\mathrm{p} & O & O \end{bmatrix}^\top \\ \boldsymbol{C}_\mathrm{vp} &= \begin{bmatrix} \boldsymbol{C}_\mathrm{p} & -2\boldsymbol{C}_\mathrm{p} & \boldsymbol{C}_\mathrm{p} \end{bmatrix} \end{aligned} \tag{15}$$

Next, the DFT $Y_{2\mathrm{diff}}(k)$ of $y_{2\mathrm{diff}}(t)$ in (14) is expressed by

$$\begin{aligned} Y_{2\mathrm{diff}}(k) &= \boldsymbol{C}_\mathrm{vp}(e^{j\omega_k}\boldsymbol{I} - \boldsymbol{A}_\mathrm{vp})^{-1}\boldsymbol{B}_\mathrm{vp}U_{2\mathrm{diff}}(k) \\ &\quad + \boldsymbol{C}_\mathrm{vp}(e^{j\omega_k}\boldsymbol{I} - \boldsymbol{A}_\mathrm{vp})^{-1}e^{j\omega_k} \\ &\quad \{\boldsymbol{x}_\mathrm{vp}(0) - \boldsymbol{x}_\mathrm{vp}(N)\} \end{aligned} \tag{16}$$

where $U_{2\mathrm{diff}}(k)$ is the DFT of $u_{2\mathrm{diff}}(t)$. When $(e^{j\omega_k}\boldsymbol{I} - \boldsymbol{A}_\mathrm{vp})^{-1}$ in (16) is expanded and rearranged using $\boldsymbol{A}_\mathrm{p}, \boldsymbol{B}_\mathrm{p}$, and $\boldsymbol{C}_\mathrm{p}$, the result is the following equation:

$$\begin{aligned} Y_{2\mathrm{diff}}(k) &= P(\omega_k)U_{2\mathrm{diff}}(k) + T_{2\mathrm{diff}}(k) \\ T_{2\mathrm{diff}}(k) &= \boldsymbol{C}_\mathrm{p}(e^{j\omega_k}\boldsymbol{I} - \boldsymbol{A}_\mathrm{p})^{-1}\left[\boldsymbol{x}_\mathrm{p}(0) - \boldsymbol{x}_\mathrm{p}(N)\right. \\ &\quad - 2\{\boldsymbol{x}_\mathrm{p}(-1) - \boldsymbol{x}_\mathrm{p}(N-1)\} \\ &\quad \left. + \boldsymbol{x}_\mathrm{p}(-2) - \boldsymbol{x}_\mathrm{p}(N-2)\right] \end{aligned} \tag{17}$$

where $T_{2\mathrm{diff}}(\omega_k)$ represents the leakage errors in ETFE-2Diff. Similar to ETFE and ETFE-Diff, the plant FRF estimate can be defined by (18) as the ratio of DFTs $U_{2\mathrm{diff}}(k), Y_{2\mathrm{diff}}(k)$ of the differential signals $u_{2\mathrm{diff}}(t), y_{2\mathrm{diff}}(t)$:

$$\hat{P}_{2\mathrm{diff}}(\omega_k) := \frac{Y_{2\mathrm{diff}}(k)}{U_{2\mathrm{diff}}(k)} = P(\omega_k) + \frac{T_{2\mathrm{diff}}(\omega_k)}{U_{2\mathrm{diff}}(k)} \tag{18}$$

From (17) and (18), the leakage-free condition in ETFE-2Diff for which $T_{2\mathrm{diff}}(\omega_k) = 0$ and $\hat{P}_{2\mathrm{diff}}(\omega_k) = P(\omega_k)$ hold is represented by

$$\begin{aligned} &\{\boldsymbol{x}_\mathrm{p}(0) - \boldsymbol{x}_\mathrm{p}(-1)\} - \{\boldsymbol{x}_\mathrm{p}(-1) - \boldsymbol{x}_\mathrm{p}(-2)\} = \\ &\quad \{\boldsymbol{x}_\mathrm{p}(N) - \boldsymbol{x}_\mathrm{p}(N-1)\} - \{\boldsymbol{x}_\mathrm{p}(N-1) - \boldsymbol{x}_\mathrm{p}(N-2)\} \end{aligned} \tag{19}$$

This equation, compared to (7) for ETFE and (10) for ETFE-Diff, shows that the time related to the leakage-free condition in ETFE-2Diff increases to six: $t = -2, -1, 0, N-2, N-1, N$. Physically, (19) implies that $T_{2\mathrm{diff}}(\omega_k) = 0$ holds when the second-order differential values (in the case of backward differential) of the plant state at $t = 0, N$ match. Furthermore, (19) is an equation including (7) for ETFE and (10) for ETFE-Diff.

TABLE II

FEASIBILITY OF LEAKAGE-FREE CONDITION IN EACH MOTION PATTERN.

Method	Leakage-free cond.	Motion pattern		
		Recip.	PTP	Ramp
ETFE ($n = 0$)	Eq. (7)	✓		
ETFE-Diff ($n = 1$)	Eq. (10)	✓	✓	
ETFE-2Diff ($n = 2$)	Eq. (19)	✓	✓	✓

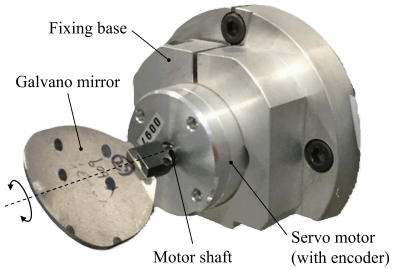

Fig. 3. Appearance of laboratory galvano scanner.

D. Feasibility of Leakage-Free Condition in Each Motion Pattern

Table II summarizes the respective feasibility of the leakage-free condition in ETFE, ETFE-Diff, and ETFE-2Diff shown in Sections III-A, III-B, and III-C for the three motion patterns (reciprocating, PTP, and ramp motions). According to the table, it is possible to suppress leakage errors across a wide range of motion patterns if the differential filtering order is increased, and accurate FRF estimation that suppresses leakage errors for all motions is theoretically possible for ETFE-2Diff. It reveals that the leakage-free condition for differential filtering order n encompasses the conditions for all orders up to $n-1$.

IV. SIMULATION-BASED COMPARATIVE EVALUATION OF FRF ESTIMATION METHODS

A. Galvano Scanner

The galvano scanner as the control object is a high-precision servo mechanism for controlling the laser position of printed circuit board laser drilling machine. It requires a response frequency of several kHz and a positioning accuracy of several μm in order to realize high productivity and machining quality. The appearance of the laboratory galvano scanner is shown in Fig. 3. The galvano scanner consists of a galvano mirror that irradiates a laser, a DC servo motor that drives the mirror, and an encoder that detects motor angular position. The dashed red line in Fig. 4 shows the measured FRF of the galvano scanner, which has resonance vibration modes at 2.83 kHz and 6.04 kHz due to motor shaft torsion and mirror deformation.

The s-domain transfer function model $P(s)$ from current reference u as the control input to motor angular position y as the control output is expressed by the following equation, considering the first and second resonance modes:

$$P(s) = K_{\mathrm{g}} e^{-Ls} \left(\frac{1}{s^2} + \sum_{i=1}^{2} \frac{k_i}{s^2 + 2\zeta_i \omega_i s + \omega_i^2} \right) \qquad (20)$$

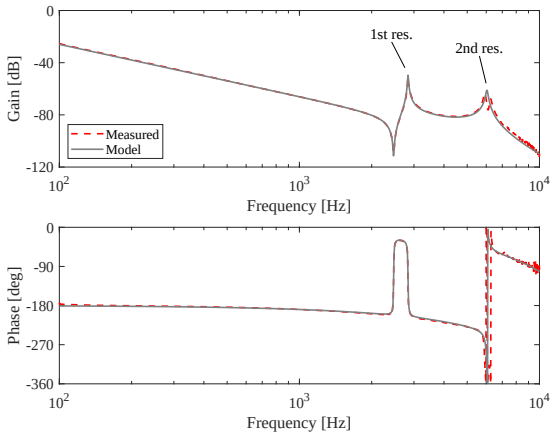

Fig. 4. Frequency response of galvano scanner.

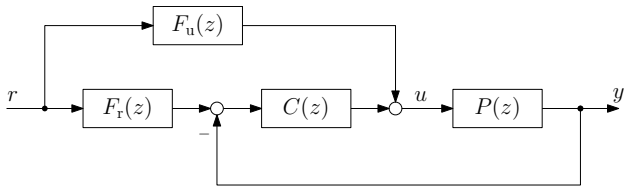

Fig. 5. Block diagram of positioning control system.

where K_{g} is the gain consisting of torque constant, moment of inertia, and steady-state gain of current control system, L is the equivalent dead time, ω_i is the resonance frequency of the i-th resonance mode, ζ_i is the damping coefficient, and k_i is the mode gain. The solid gray line in Fig. 4 shows the model FRF of $P(z)$, which is obtained by discretizing $P(s)$ via the Tustin transformation with sampling period $T_{\mathrm{s}} = 20$ μs. The model FRF well reproduces the measured FRF.

B. Positioning Control System

Fig. 5 shows a block diagram of a two-degree-of-freedom positioning control system used for simulation evaluation. In the figure, r denotes the target position reference, $P(z)$ is the plant, $F_{\mathrm{r}}(z)$ and $F_{\mathrm{u}}(z)$ denote FF controllers, and $C(z)$ is the feedback (FB) controller. The control period is $T_{\mathrm{s}} = 20$ μs. The FF controllers were designed based on the coprime factorization framework using $P(z)$ and a sixth-order low-pass filter whose cut-off frequency of 3000 Hz. On the other hand, the FB controller was designed using a PID compensator and two second-order all-pass filters for resonance mode compensation so that the gain cross over frequency of the open-loop became about 830 Hz.

C. Simulation Condition

Table III shows the maximum stroke, maximum speed, and maximum acceleration used in the design of position reference $r(t)$ for reciprocating, PTP, and ramp motions, while Fig. 6 shows the waveforms of the designed $r(t)$ for all motion patterns. In the simulation described below, $u(t)$ and $y(t)$ (plant input and output signals) obtained by each motion were used to perform FRF estimation by ETFE,

TABLE III

SETTINGS OF POSITION REFERENCE.

Parameter	Recip.	PTP	Ramp
Max stroke [rad]	6.58×10^{-3}	6.58×10^{-3}	0.33
Max vel. [rad/s]	40	40	40
Max acc. [rad/s^2]	500×10^3	500×10^3	500×10^3

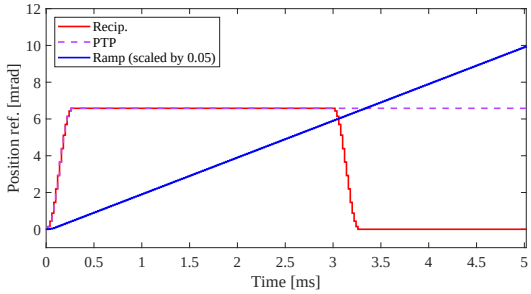

Fig. 6. Response waveform of position reference $r(t)$.

ETFE-Diff, and ETFE-2Diff, and the estimation accuracy was then compared and evaluated. Furthermore, the data length of the input and output signals was set to $N = 251$ ($NT_\mathrm{s} = 5.02$ ms), and for the DFT, considering the frequency resolution, zero-padding was applied to the end of the data to set the data length to $M = 4096$ ($NT_\mathrm{s} = 81.92$ ms). In addition, in order to isolate the cause of FRF estimation errors to solely leakage errors, the simulation disregarded quantization of the output signal, disturbance, and noise.

Figs. 7, 8, and 9 show the response waveform of control input $u(t)$, motor angular position $y(t)$, and their differential values $u_\mathrm{diff}(t), y_\mathrm{diff}(t), u_\mathrm{2diff}(t), y_\mathrm{2diff}(t)$ in each motion. It is evident that the assumptions listed in Table I are almost ideally satisfied for each motion pattern (although waveforms at $t < 0$ are not shown, $\boldsymbol{x}_\mathrm{p}(t < 0) = \boldsymbol{x}_\mathrm{p}(0) = \boldsymbol{O}$ is strictly satisfied).

D. FRF Estimation Results

Fig. 10 shows the FRF estimation results for reciprocating motion. In all the FRF estimation methods, the FRF estimates closely matched the true FRF. Furthermore, while the absolute amount was not substantial, an increase of the differential filtering order n led to an increase of the low-frequency estimation error. This phenomenon was also observed under subsequent evaluation conditions, indicating that it was due to the assumptions in Table I not being strictly met. Fig. 11 shows the FRF estimation results for PTP motion. Although a highly accurate FRF estimates were obtained using ETFE-Diff and ETFE-2Diff, ETFE incurred significant FRF estimation errors produced by the leakage errors. Finally, Fig. 12 shows the FRF estimation results for ramp motion. In this motion pattern, only ETFE-2Diff satisfied the leakage-free condition, and accurate FRF estimation was realized.

From the above simulation results, it can be concluded that increasing the differential filtering order enables FRF

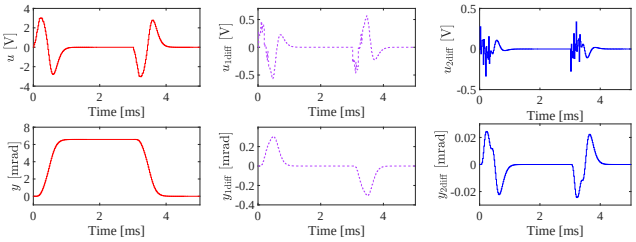

(a) (b) (c)

Fig. 7. Waveforms of time responses in *reciprocating* motion: (a) $u(t)$, $y(t)$; (b) $u_\mathrm{1diff}(t)$, $y_\mathrm{1diff}(t)$; (c) $u_\mathrm{2diff}(t)$, $y_\mathrm{2diff}(t)$.

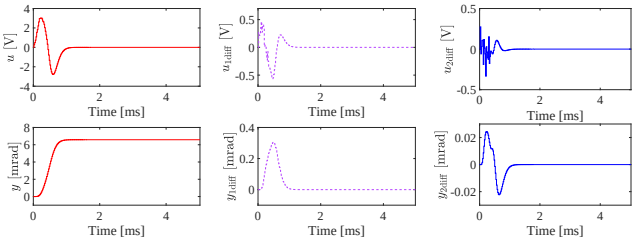

(a) (b) (c)

Fig. 8. Waveforms of time responses in *PTP* motion: (a) $u(t)$, $y(t)$; (b) $u_\mathrm{1diff}(t)$, $y_\mathrm{1diff}(t)$; (c) $u_\mathrm{2diff}(t)$, $y_\mathrm{2diff}(t)$.

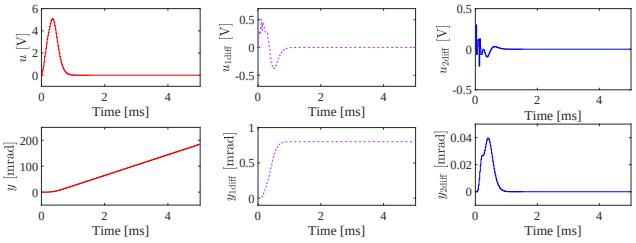

(a) (b) (c)

Fig. 9. Waveforms of time responses in *ramp* motion: (a) $u(t)$, $y(t)$; (b) $u_\mathrm{1diff}(t)$, $y_\mathrm{1diff}(t)$; (c) $u_\mathrm{2diff}(t)$.

estimation with reduced leakage errors over a broader range of motion patterns. This demonstrates the validity for Table II as theoretically presented in Sect. III-D.

V. CONCLUSION

In this paper, we performed theoretical analyses and simulation evaluations to investigate the relationship between the leakage-free condition and the order of differential filtering in FRF estimation methods that incorporate ETFE with differential filtering. The leakage-free condition for ETFE-2Diff was theoretically derived, comparing to the existing ETFE and ETFE-Diff, and it was found that increasing the differential filtering order extends the leakage-free conditions, which enabled accurate FRF estimation in a broader motion patters. Furthermore, the validity of the theoretical considerations was verified through FRF estimation simulations for reciprocating, PTP, and ramp motions.

This paper did not consider the influence of nonlinearity and external disturbance or noise, which could have adverse effects in ETFE with differential filtering. The theoretical

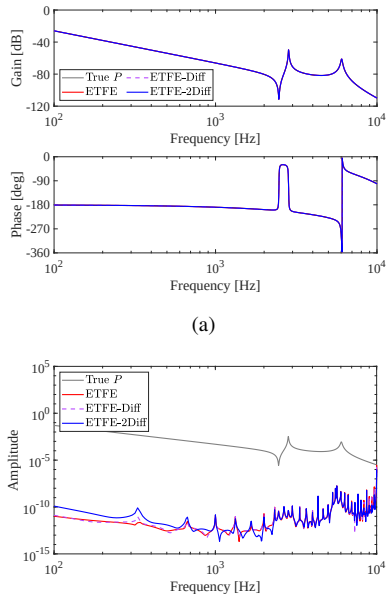

Fig. 10. FRF estimation results in *reciprocating* motion: (a) $\hat{P}_{0\mathrm{diff}}(\omega_k)$; (b) $|P(\omega_k) - \hat{P}_{0\mathrm{diff}}(\omega_k)|/|P(\omega_k)|$.

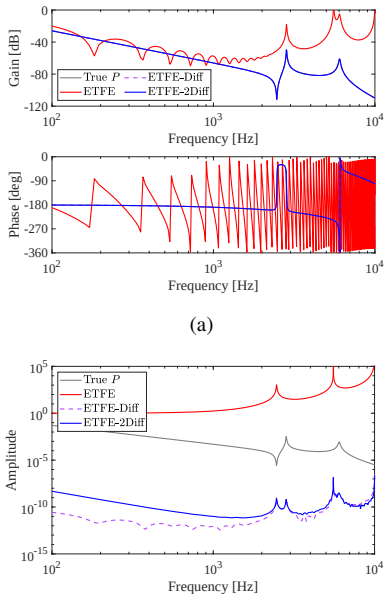

Fig. 11. FRF estimation results in *PTP* motion: (a) $\hat{P}_{1\mathrm{diff}}(\omega_k)$; (b) $|P(\omega_k) - \hat{P}_{1\mathrm{diff}}(\omega_k)|/|P(\omega_k)|$.

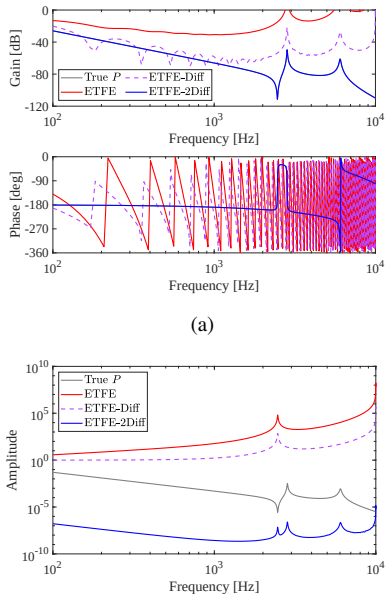

Fig. 12. FRF estimation results in *ramp* motion: (a) $\hat{P}_{2\mathrm{diff}}(\omega_k)$; (b) $|P(\omega_k) - \hat{P}_{2\mathrm{diff}}(\omega_k)|/|P(\omega_k)|$.

analysis and evaluation regarding these aspects are subjects for future research.

REFERENCES

[1] M. Steinbuch, T. Oomen, and H. Vermeulen, "Motion control, mechatronics design, and Moore's law," *IEEJ Jour. Ind. App.*, vol. 11, no. 2, pp. 245–255, 2022.

[2] Y. Maeda and M. Iwasaki, "A command shaping approach for suppressing scattered responses on servo systems with rolling friction," in *Proc. 2018 IEEE/ASME Int. Conf. Adv. Intel. Mechatron.*, TuBT2.2, pp. 244-249, 2018.

[3] E. Evers, R. Voorhoeve, and T. Oomen, "On frequency response function identification for advanced motion control," in *Proc. IEEE 16th Int. Workshop Adv. Motion Control*, pp. 319–324, 2020.

[4] C.K. Pang and F.L. Lewis, "System identification of modal parameters in dual-stage hard disk drives," in *Proc. IEEE Int. Conf. Control Automat.*, pp. 603–608, 2018.

[5] Y. Maeda, S. Kunitate, E. Kuroda, and M. Iwasaki, "Autonomous cascade structure feedback controller design with genetic algorithm-based structure optimization," in *Proc. 21st IFAC World Congress*, pp. 8529–8535, 2020.

[6] R. de Rozario, A. Fleming, and T. Oomen, "Finite-time learning control using frequency response data with application to a nanopositioning stage," *IEEE/ASME Trans. Mechatron.*, vol. 24, no. 5, pp. 2085–2096, 2019.

[7] J. Schoukens, G. Vandersteen, K. Barbé, and R. Pintelon, "Nonparametric preprocessing in system identification: A powerful tool," in *Proc. Eur. Control Conf.*, pp. 1–14, 2009.

[8] A. Mamatov and S. Lovlin, "Experimental estimation of frequency response functions of precision servo drive systems," in *Proc. 2018 X Int. Conf. Electric. Power Drive Syst.*, 2018.

[9] T. McKelvey and G. Guérin, "Non-parametric frequency response estimation using a local rational model," in *Proc. 16th IFAC Symp. Syst. Ident.*, pp. 49–54, 2012.

[10] J. Schoukens, K. Godfrey, and M. Schoukens, "Nonparametric data-driven modeling of linear systems: Estimating the frequency response and impulse response function," *IEEE Control Systems Mag.*, vol. 38, no. 4, pp. 49–88, 2018.

[11] H. Sekine, S. Ueda, M. Suzuki, and M. Hirata, "System identification of a galvano dcanner using input-output data obtained from positioning control," in *Proc. Eur. Control Conf.*, pp. 1297–1302, 2015.

[12] H. Tachibana, N. Tanaka, Y. Maeda, and M. Iwasaki, "Comparisons of frequency response function identification methods using single motion data: Time- and frequency-domain approaches," in *Proc. IEEE Int. Conf. Mechatron.*, pp. 498–503, 2019.

[13] Y. Maeda and M. Iwasaki, "Empirical transfer function estimation with differential filtering and its application to fine positioning control of galvano scanner," *IEEE Trans. Ind. Electron.*, vol. 70, no. 10, pp. 10466–10475, 2023.

[14] Y. Maeda and M. Iwasaki, "Frequency-domain modeling-free iterative learning control for point-to-point motion," in *Proc. 32nd IEEE Int. Symp. Ind. Electron.*, ISIE23-000213, 2023.